lement d'un ecoulement supersonique," Proceedings of the 10th International Congress of Applied Mechanics, Stresa, Italy (September 1960).

[13] Karashima, K., "Base pressure on two-dimensional blunt-trailing-edge wings at supersonic velocity," University of Tokyo, Aeronautical Research Inst. Rept. 368 (October 1961).

[14] Thomann, H., "Measurements of heat transfer and recovery temperature in regions of separated flow at a Mach number of 1.8," The Aeronautical Research Institute of Sweden F.F.A. Rept. 82 (1959).

[15] Badrinarayanan, M. A., "An experimental investigation of base flows at supersonic speeds," J. Roy. Aeronaut. Soc. **65**, 475–482 (1961).

[16] Roshko, A. and Thomke, G. J., "Flow separation and reattachment behind a downstream-facing step," Douglas Aircraft Co. Rept. SM-43056-1 (1964).

[17] Charwat, A. F. and Yakura, J. K., "An investigation of two-dimensional supersonic base pressure," J. Aerospace Sci. **25**, 122–128 (1958).

Production of Supersonic Flows with Honeycomb-Supported Screens

H. N. Powell,* R. K. Suri,† and W. G. Steenken‡
University of Wisconsin, Madison, Wis.

Introduction

In the course of a special shock-tube development program,§ the performance characteristics of honeycomb-supported screens for the production of supersonic flows was investigated using air and argon. Screens may be considered a variant form of the multinozzle that has been studied by several authors.[1,2] The principal advantages of the screen are its mechanical simplicity, the possibility of producing disturbance-free flows, and, relative to the nozzle, the very short flow-stabilization time for large-diameter ducts. The last feature is especially important for blow-down applications, as in the authors' case.

The only previous work, that of Gould,[3] shows the existence of substantial radial flow components emerging from the screen, as is evidenced by the pronounced shock diamonds, which caused the local Mach number to vary as much as 0.35 across the stream. The radial components can be attributed either to mechanical distortion of the screen or a convection through it of radial momentum produced by the flattening effect of the screen on the incoming velocity profile. Presumably because of strength limitations, Gould used quite coarse screens (9 to 20 mesh/in.) that gave a clearly visible fixed pattern of disturbances for several inches or more downstream. Unsteady fluctuations undoubtedly extended much further.

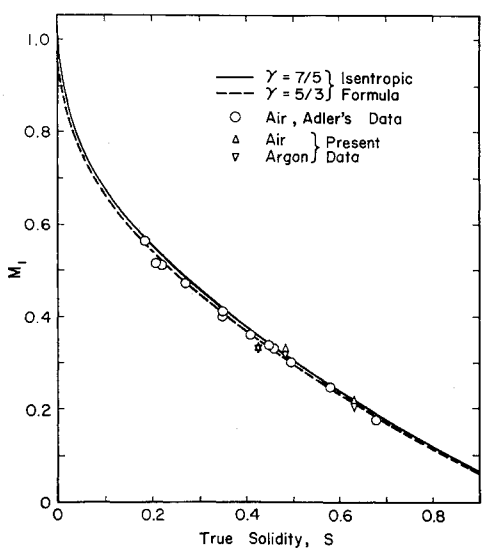

Fig. 1 Inlet Mach number as a function of true solidity.

By means of a simple structural modification, resistance-welding a stainless-steel screen to the downstream side of a layer of stainless-steel honeycomb, the present authors have eliminated these difficulties. Two objectives are served thereby: 1) the honeycomb eliminates radial momentum coming into the screen; and 2) the closely spaced local support holds the screen flat and permits a much finer mesh screen to be used, resulting in a correspondingly finer scale and less persistent downstream disturbance pattern. These advantages are purchased with somewhat increased total pressure losses and a decreased maximum Mach number. The discussion falls naturally under the three major divisions.

Upstream Flow State and Mass Flow Rate

Adler[4] and Cornell[5] state that the (choked flow) upstream Mach number M_1 is determined by the screen solidity (= blocked area/total area) and the isentropic choked flow formula. However, at high solidities, Adler's M_1 data are as much as 10% higher by this criterion. Since frictional effects cannot account for a change in this direction, it must be attributed to a somewhat increased "true" flow area relative to that which they computed. If a "wire-cloth" screen (i.e., both warp and fill wires have sine wave shapes) is made of wire of diameter d with a mesh m, the maximum and mean displacements from the center of one wire to the next are d and $d/2^{1/2}$, respectively, so that the aperture area is approximately $[(1/m^2 + 1/2d^2)^{1/2} - d]^2$ instead of $[1/m - d]^2$. With the "bolting-grade" screen in which one family of wires is straight, the maximum and mean normal displacements of the curved wires are $2d$ and $2^{1/2}d$, respectively, giving an aperture area of $[(1/m^2 + 2d^2)^{1/2} - d][1/m - d]$. The "normal" and "true" solidities of single screens are then

$$S_n = 1 - [1 - md]^2 \text{ "normal" solidity, any screen or square-cell honeycomb} \quad (1a)$$

$$S_{ts} = 1 - \{[1 + \tfrac{1}{2}(md)^2]^{1/2} - md\}^2 \text{ wire-cloth screen} \quad (1b)$$

$$S_{ts} = 1 - \{[1 + 2(md)^2]^{1/2} - md\}[1 - md] \text{ bolting-grade screen} \quad (1c)$$

By similar reasoning, and using the honeycomb m and d in Eq. (1a), the effective honeycomb solidity in the plane of the screen is estimated to be $S_h = 0.6\,S_n$. The combined solidity and its relation to the area-ratio function A/A^* is

$$S = S_{ts} + S_h(1 - S_{ts}) = 1 - A^*/A \quad (2)$$

Table 1 Solidity data

	Mesh m, in.$^{-1}$	Wire diam d, in.	Normal solidity S_n, Eq. (1)	True solidity S_{ts}, Eq. (1)	Combined solidity S, Eq. (2)
Honeycomb	4	0.0060	0.048	0.029	...
Wire-cloth screen	40	0.0060	0.423	0.401	0.420
Bolting-grade screen	20	0.0162	0.543	0.475	0.491
Wire-cloth screen	60	0.0072	0.678	0.621	0.633

Received October 2, 1964; revision received March 22, 1965.
* Professor of Mechanical Engineering. Member AIAA.
† Research Assistant; now at University of Roorkee, India.
‡ Research Assistant.
§ Supported in part by the National Science Foundation.

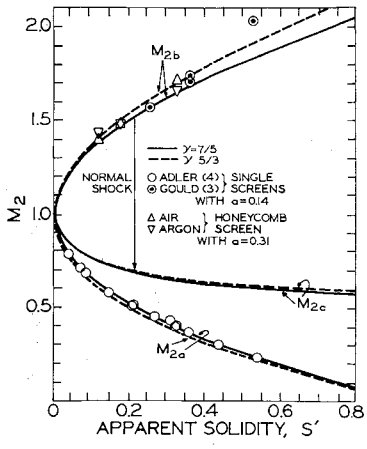

Fig. 2 Equation (5) correlation of data as a function of apparent solidity, $S' = S - a$.

(To avoid interference effects, the screen wires should not be parallel to the honeycomb walls.) In the absence of a honeycomb, $S_h = 0$.

Figure 1 shows a satisfactory agreement between the standard isentropic area-ratio formula $M = f(A/A^*)$ and the observed M_1's of both Adler[4] and the present authors. The aerodynamic effects of the corrections from normal to true solidity can be judged from the graph and the S_n and S_{ts} columns of Table 1. It is therefore concluded that, for both Adler's single-screen and the present honeycomb-screen experiments, the flow is isentropic to $M = 1$, and all losses occur on the downstream side. (Reynolds number effects are discussed under the last heading.)

Downstream Flow States

Let a control surface be located through the midplane of the screen, where the flow is regarded as choked, and a second surface of the same shape and total area be located in a downstream uniform flow state 2. To apply the one-dimensional momentum equation, let the back pressure on the screen be $S'P_2$, in which S', an "apparent solidity," is related to S by

$$S' = S - a \tag{3}$$

The momentum equation now becomes

$$P^*(1 - S)(1 + \gamma) + P_2S' = P_2(1 + \gamma M_2^2) \tag{4}$$

The value $a = 0$ corresponds to a limiting case of an instantaneous transition to state 2 after $M = 1$. By eliminating P_2/P^* and T_2/T^* between Eq. (4) and the continuity and adiabatic energy equations, a solution for M_2^2 is obtained:

$$M_2^2 = (1 + \gamma S')\{1 \pm [1 - (1 - S')^2/(1 + \gamma S')^2]^{1/2}\} \tag{5}$$

Figure 2 shows an excellent correlation of Eq. (5) with all existing data. The value $a = 0.14$ correlates both Adler's[4] $M_{2a} < 1$ data with the minus root and, despite the presence of shocks, three out of four of Gould's[3] $M_{2b} > 1$ data with the plus root. The value $a = 0.31$ correlates the present $M_{2b} > 1$ data. Also shown is the M_{2c} curve, which is related to the M_{2b} curve by the normal shock relations. The M_{2c} and M_{2a} curves, therefore, bound a condition of partial shock penetration of the screen. Figure 3 shows the total pressure ratio curves corresponding to the M_{2a} and M_{2b} data of Fig. 2. Since P_{02}/P_{01} depends on both S and S', no single correlation is possible. The mechanism that accounts for the greater honeycomb-screen losses is discussed at the end of the note.

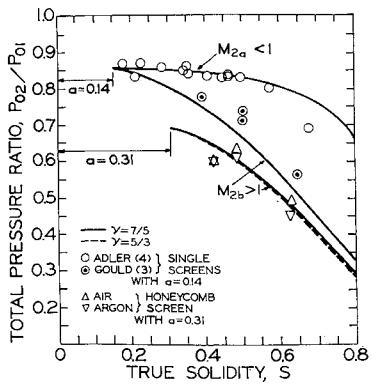

Fig. 3 Correlation of experimental total pressure ratios with curves based on Eq. (5).

Experimental Background and Reynolds Number Range

Screen data are given in Table 1. The performance data were obtained from pressure measurements (the Kistler transducers were calibrated daily) in a blow-down apparatus that gave steady flow conditions through the screen for 15 msec. Cylinder (i.e., dry) air and argon were used. Four to six tests were made for each set of conditions. The duct diameter was 6.30 in., and the honeycomb was 3.00 in. thick.

M_{2b} was obtained directly from wall and pitot transducer measurements in a plane 6.00 in. (240 to 360 mesh sizes) downstream of the screen. This plane was chosen to facilitate detection of oblique shocks, if present, by pitot measurements at the center and half-radius positions; none were detected as the readings were the same. Rotation of the screen also gave no effect. Submicrosecond schlieren photographs taken in the test section 3 ft downstream showed the flow to be free of extraneous Mach disturbances and visible turbulence. The ΔP across the unsteady expansion upstream of the honeycomb was too small for a sufficiently accurate determination of M_1; instead, M_1 was calculated with the Fanno functions from M_{2b} and P_{2b}/P_1 static pressure ratio data. All pressure ratios were independent of the pretest downstream diaphragm pressure.

With a screen Reynolds number defined by $Re = (1/m - d)\rho^*c/\mu^*$, Adler's data fall between 2.5×10^4 and 9.0×10^4, Gould's between 1.2×10^4 to 2.9×10^4, and the present data of Figs. 1–3 between 6.4×10^3 and 2.7×10^4. Thirty-eight additional air tests were made with the $S = 0.633$ screen to study viscous effects. Considering the measurement problems at low pressures, no clear deviations from the data of Figs. 1–3 for this screen were detected to $Re = 9.5 \times 10^2$ at $P_1 = 18$ cm Hg. The largest change was an increase in P_1/P_{2b} from 10.0 ± 0.2 (max) to 10.9 ± 0.9 (max) at $Re = 9.5 \times 10^2$. (The wall transducers gave P_1/P_{2b} data throughout this range, but the small-area pitot transducer could not be used below $P_1 = 40$ cm Hg; within the measured range, M_{2b} was quite constant.) It is therefore concluded that viscous effects are not significant in the range $9.5 \times 10^2 < Re < 2.9 \times 10^4$. However, at $Re = 3.9 \times 10^2$, P_1/P_{2b} fell sharply to 9.0 ± 0.8 (max). A transition regime for $Re \leqslant 8 \times 10^2$ is consistent with Cornell's[5] curves from incompressible data.

Special note should be taken of the honeycomb-screen performance sensitivity to upstream flow conditions. In certain instances a slight scoring and bending of the inlet edges of the honeycomb caused markedly increased total pressure losses. Even if the uncertainties of Gould's data are allowed for, it is clear that the honeycomb-screen losses are markedly greater. This is not directly attributable to the honeycomb, since the total pressure losses in it are negligible throughout the entire Reynolds number range investigated, as is supported by Fig. 1. However, in light of the preceding observation, it can be attributed to the sensitivity of the screen performance to turbulence produced on the walls and inlet edges of the honeycomb. Greater losses, therefore, are the price of the flow uniformity that the honeycomb provides.

References

[1] Royle, J. K., Bowling, A. G., and Lukasiewicz, J., "Calibration of two dimensional and conical supersonic multi-nozzles," Rept. Aero. 2221, S. D. 23, Royal Aircraft Establishment (September 1947).

[2] Reshotko, E. and Haefeli, R. C., "Investigation of axially symmetric and two-dimensional multi-nozzles for producing supersonic streams," NACA RM E52H28 (1952).

[3] Gould, L. I., "Preliminary investigation of the supersonic flow field downstream of wire-mesh nozzles in a constant-area duct," NACA RM E51F25 (1951).

[4] Adler, A. A., "Variation with Mach number of static and total pressures through various screens," NACA Wartime Rept. L-23; originally issued as Confidential Bull. L5F28 (February 1946).

[5] Cornell, W. G., "Losses in flow normal to plane screens," Trans. Am. Soc. Mech. Engrs. **80**, 791–799 (1958).

Exhaust Measurements on the Plasma from a Pulsed Coaxial Gun

D. E. T. F. Ashby,* T. J. Gooding,†
B. R. Hayworth,‡ and A. V. Larson§
General Dynamics/Astronautics, San Diego, Calif.

Introduction

Although several groups have investigated pulsed plasma guns for electric propulsion,[1–4] exhaust measurements have been limited mainly to the determination of gross parameters such as total energy content and momentum.[5] More detailed information on the exhaust characteristics is desirable for a better understanding of the acceleration mechanisms. A simple technique of measuring ion current is described with which ion densities up to 3×10^{13} cm^{-3} and ion velocities from 10^6 to 10^7 cm-sec^{-1} have been determined as a function of time and position in the nitrogen plasma from a coaxial gun. The technique has been used previously on high energy hydrogen plasmas produced by guns used in controlled thermonuclear research;[6,7] it is similar to a technique used for examining ion beams.[8]

Description of the Apparatus

The coaxial gun used has been described elsewhere;[3] it produces a burst of nitrogen plasma, containing approximately 10^{18} ions, which travels at several centimeters per microsecond. The probe used to measure ion current is a negatively biased Faraday cup completely surrounded by a grounded shield containing a small entrance hole for the plasma and several pumping holes to ensure that the neutral particle density inside the probe is low. Diagrams of the probe and the biasing circuit are shown in Fig. 1, together with a typical oscillogram of the probe output. The probe is mounted so that it can be moved to different positions in the exhaust.

The cup is biased sufficiently negative so that all the electrons in the plasma which enter the probe are repelled from the cup while the ions are collected. For a plasma of predominately one ion species, the amplitude of the ion current collected (I) is

$$I = nev\,AZ \qquad (1)$$

Presented as Preprint 64-705 at AIAA Fourth Electric Propulsion Conference, Philadelphia, Pa., August 31–September 2, 1964; revision received January 14, 1965. This work was supported by NASA on Contract No. NAS 3-2594.

* Consultant, Space Science Laboratory; on leave of absence from Culham Laboratory, England.

† Senior Staff Scientist, Plasma Propulsion Group, Space Science Laboratory. Member AIAA.

‡ Staff Scientist Plasma Propulsion Group, Space Science Laboratory. Member AIAA.

§ Staff Scientist, Plasma Propulsion Group, Space Science Laboratory.

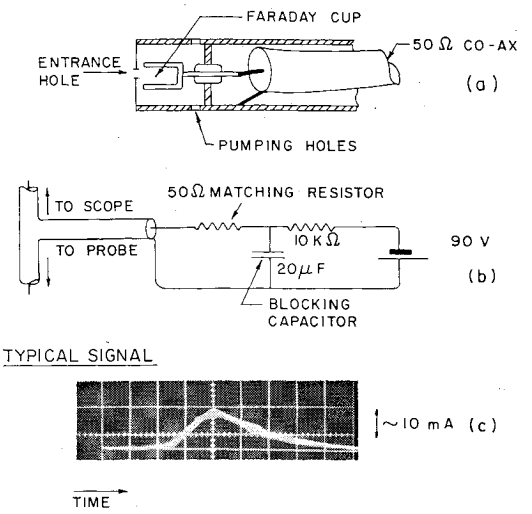

Fig. 1 a) Ion probe; not to scale; over-all diameter 1.5 cm. b) Biasing circuit. c) Typical signal, 8 trace overlay; 5 μsec/cm, flight distance 136 cm, entrance hole 0.5-mm diam.

where n is the ion number density, e is the electronic charge, v is the component of ion velocity normal to the face of the probe, A is the area of the entrance hole, and Z is the number of electronic charges per ion.

If the flight distance is much greater than the gun length and if the transit time greatly exceeds the electrical period, then the plasma can be considered as originating from a point source; therefore, the velocity v of the plasma can be calculated from the time of flight. With v known, nZ is obtained from the amplitude of the ion current. For example, the oscillogram in Fig. 1 shows that the plasma corresponding to the peak in ion current arrives at the probe with a velocity of 6.5 cm/μsec and, if singly ionized, has an ion density of 6.5×10^{12} cm^{-3}.

Experimental Results

The bias voltage necessary to repel electrons from the ion collector is two or three times the electron temperature in electron volts plus any potential difference between the outer

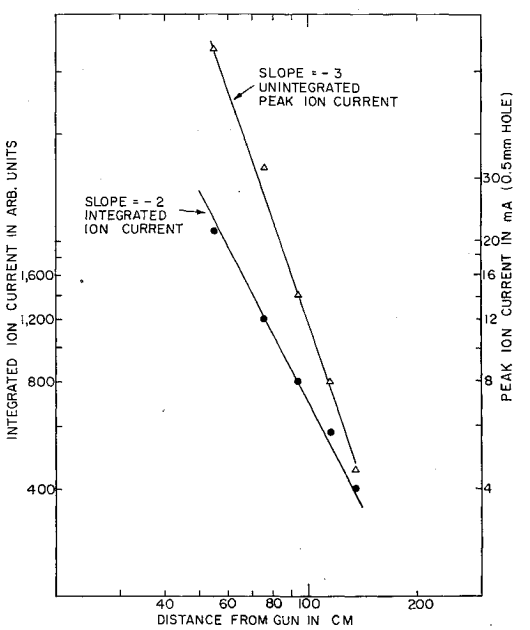

Fig. 2 Probe ion current vs distance from the gun. Gun operating conditions differ from those for Fig. 1c.